2010

Frequency and load mode dependence of Vibrothermography

Wenjun Zhang
Iowa State University

Frequency and load mode dependence of Vibrothermography

by

Wenjun Zhang

A thesis submitted to the graduate faculty

in partial fulfillment of the requirements for the degree of

MASTER OF SCIENCE

Major: Engineering Mechanics

Program of Study Committee:
Stephen D. Holland, Major Professor
R. Bruce Thompson
Thomas J. Rudolphi

Iowa State University

Ames, Iowa

2010

TABLE OF CONTENTS

LIST OF TABLES iv

LIST OF FIGURES v

ACKNOWLEDGEMENTS viii

ABSTRACT ix

INTRODUCTION 1

FREQUENCY DEPENDENCE OF VIBROTHERMOGRAPHY 3

Abstract 3

Introduction 3

Theory 4

Experiment 5

Results 7

Conclusions 12

Acknowledgements 14

DEPENDENCE OF VIBROTHERMOGRAPHIC HEATING ON SHEAR VERSUS NORMAL LOADING 15

Abstract 15

Introduction 15

Theory 17

Experiment 18

Results 22

Conclusions 25

Acknowledgements 26

APPENDIX: PROCEDURE OF GROWING MULTIPLE CRACKS ON ONE SPECIMEN 27

Introduction 27

Step-by-step procedure 28

Summary 29

BIBLIOGRAPHY 32

LIST OF TABLES

Table 1 Cracks length characteristics in Set A and Set B (all lengths are in mm) 6

Table 2 Estimated parameters from statistical models, with standard error . . 12

Table 1 Size of EDM notches and final length of cracks of specimen B1 and B2 (all lengths are in mm) 30

LIST OF FIGURES

Figure 1 Crack locations of specimen in Set B. Thirteen notches (bold lines in the figure) were made. Five center cracks and eight off center cracks. . 6

Figure 2 Experimental setup used for exciting the test specimens and observing heat generation. 8

Figure 3 Comparison of surface velocity profile between laser vibrometer scanning and finite element simulation at different resonance modes. 9

Figure 4 Comparison of stress/displacement ratio between flexural beam theory and finite element simulation. (a) has the same geometry as the specimens in Set A, while (b) has half the thickness, which makes the resonance frequency lower and the result from flexural beam theory matches that from finte element. 10

Figure 5 A typical vibrothermographic heating recorded by the calibrated infrared camera. This is specimen B2 from Set B. 10

Figure 6 Heating versus dynamic normal stress at two different resonances. These two specimens are A119 and A124 from Set A. 11

Figure 7 Heating versus dynamic normal stress at different resonances. These two cracks were B1_12 on specimen B1, and B2_13 on specimen B2 from Set B. 11

Figure 8 3-D plots of the measured data points and the fitted surface. (a) shows the data from Set A, at two different resonances. (b) shows the data from Set B, at three different resonances. 13

Figure 1 A typical 1.2 mm fatigue crack under optical microscopy (left) and the sketch of the contacting asperities (right). The local orientation is different in each of the contacting asperities. The remote stress is then decomposed into normal and shear component in these local contacting asperities. 17

Figure 2 Specimen with multiple initial EDM notches and fatigue cracks. There are five center notches and eight off center notches on each specimen. Horizontal distance between the neighboring two notches is 25.4 mm and the vertical distance between two notches is 12.7 mm. Fatigue cracks were grown from these notches. 19

Figure 3 Flexural resonances in two directions. Vibration shown in (a) is in the Y direction, and the color is mapped from dynamic shear stress. Vibration in (b) is in Z direction (out of the paper), and the color is mapped from dynamic normal stress. 20

Figure 4 Experimental setup in this study. Piezoelectric transducer excites the flexural vibration in the vertical direction, motions were measured by laser vibrometers, and the heating was recorded by the infrared camera. 21

Figure 5 Heating of the vibrometer tape. Tapes were stuck to the top and the bottom of the specimen. This heating pattern indicates the 5th order flexural resonance mode. The two brigher spots at the bottom of the specimen were rubber pins, which were placed at the nodal points. . . 22

Figure 6 Vibrothermographic heating from cracks in specimen B1. Five cracks can be identified from this figure, but only the one in the middle was under pure shear dynamic stress. 23

Figure 7 Vibrothermographic heating from cracks in specimen B2. Ten cracks can be identified from this figure, and the three along the center line were under pure shear dynamic stress. 23

Figure 8 Temperature rises of the four center cracks versus dynamic shear stresses. Y axis in the plot is the temperature corrected by frequency, e.g. $\Delta T/f^{0.88}$. 25

ACKNOWLEDGEMENTS

I would like to thank my advisor, Prof. Stephen D. Holland, for his support and encouragement to complete this work. He gave me an opportunity to learn and research, and guided me with extreme patience.

I would also like to express my gratitude to the members of my thesis committee: Prof. R. Bruce Thompson and Prof. Thomas J. Rudolphi, for their review and valuable comments.

I would like to take this opportunity to express my thanks to those who helped me in my graduate study in Iowa State University. They are Prof. Thomas J. Rudolphi, Prof. Lester W. Schmerr, Prof. Ashraf Bastawros, Prof. Aleksandar Dogandžić, Prof. Jue Yan, Prof. Alric Rothmayer, Ms. Delora Pfeiffer, Ms. Heidi Long, and many others.

I am indebted to my peers in the Department of Aerospace Engineering and Center for NDE, De Huang, Hui Wang, Jeremy Renshaw, Jyani Vaddi, Ricky Reusser, Ying Zhou and many others.

My fiancée Tiky and my parents have always stood by me, without their support I would not have been able to complete this work.

ABSTRACT

Vibrothermography is a method for finding cracks based on the heat generation due to vibration-induced rubbing of the crack surfaces. This technique has shown substantial promise for industrial use finding flaws in gas turbine parts, but the underlying physics remains unclear. Two long standing questions are the dependence of crack heating on excitation frequency, and the dependence of crack heating on loading mode (normal vs shear). With our broadband excitation system, we are able to excite the specimen at different resonances, and correlate the heating with dynamic vibrational stress and frequency of vibration. By exciting the specimen in different modes that load a particular crack either in pure normal stress or pure shear stress, we can measure how crack heating depends on loading mode. Our data shows that similar amount of heating occurs due to normal and shear stresses. In addition, when we fit a simple power law to the heating versus dynamic stress, we found that characteristics of different types of loading seem to be quite similar. A more general physical model is then proposed, which incorporates the dependence of vibrational frequency and dynamic loading types.

INTRODUCTION

Vibrothermography, also known as Sonic IR or Thermosonics, is a method for finding cracks based on heat generation due to the vibration-induced frictional rubbing the crack asperities[1]. This technique has shown substantial promise for industrial use finding flaws in gas turbine parts, but the underlying physics remains unclear. Many research groups around the world working on Vibrothermography only focus on its applications, as opposed to make a systematic study of the mechanism inside it, which no only limits the broader usage of this technique, but also makes some experimental results empirical or even superficial. What we are trying to do is to investigate every possible factor in the heat generation and detection, and fuse the individual pieces of information to obtain a general heating function.

We knew that the vibration of the specimen is dominated by resonance effects, and realizing this idea, we were able to obtain the same heating of cracks (which were usually achieved with ultrasonic welder in the past) with a much less power broadband piezoelectric transducer working exactly at the natural resonances of the specimen. The switch from mono-tone ultrasonic welder to broadband excitation system is substantial because it enables us to control the vibration as we want. With the broadband excitation system, some of the important factors involved in the heat generation and detection process have been identified and investigated by the members of our group. For example, dynamic normal stress and crack length have been found directly link to the amount of heat generated[2]. Two other factors have long been postulated to effect the heat generation process as well: vibrational frequency and loading mode, i.e. normal and shear. Here we are trying to understand the influence of these two factors by designed experiments and physical models. It is almost impossible for someone who uses narrow band excitation system to answer such questions.

When specimens are vibrating at resonances, changing the excitation frequency changes the resonance mode, as well as the internal stress status. Since the vibrational frequency and dynamic stress are coupled in this problem, the way to tackle it is measuring heating, stress[3] and frequency at the same time for each excitation, and doing the surface fitting of temperature increase in space of frequency and dynamic stress. While the same basic ideas and methodology are also applicable to the study of dependence on loading type (normal and shear), the most difficult and time-consuming part is to find the suitable specimen geometry and resonance modes, where cracks are under pure shear loading, and the loading is high enough to generate detectable temperature increase. We have tested different shapes, such as square and rectanglar plates, bars with different lengths and cross-sections, and finally we seleted long slender bars with the dimension of 310 mm $\times$ 25.4 mm $\times$ 6.1 mm.

After we collected the data matrix (Heat, Stress and Frequency), we fitted the data with a power law model, which assumes that temperature increase is power function of dynamic stress and frequency, i.e. $\Delta T = A\sigma^{\alpha} f^{\beta}$. In the frequency dependence study, σ was dynamic normal stress, and parameters A, α and β were estimated. In the modal dependence study, σ was dynamic shear stress and the corresponding A and α were estimated. We also proposed a physical model base the experimental evidence.

The thesis is composed of two papers that to be submitted, and an appendix which describes the procedure of growing multiple cracks on the single specimen.

FREQUENCY DEPENDENCE OF VIBROTHERMOGRAPHY

A paper to be submitted to Journal of NDE

Wenjun Zhang and Stephen. D Holland

Abstract

It has long been postulated that vibrothermographic heating—the heating of cracks due to sound or vibration-induced rubbing—may be frequency dependent. It has been difficult to factor out the innate frequency dependence of the heat-generation process from the geometry-dependent mode structure. We present experiments showing that heating of cracks in slender Inconel/Titanium bars at transverse resonance. Different resonance modes vibrate at different frequencies but load the crack in the same way (Mode I). The results show a clear increase of heating with vibration frequency.

Introduction

Vibrothermography is a method for finding cracks based on heat is generated due to vibration-induced frictional rubbing the crack asperities[1]. This technique has shown substantial promise for industrial use finding flaws in gas turbine parts, but the underlying physics remains murky. One longstanding question is how the amount of crack heating depends on the frequency of vibration. Specimens can be excited at predetermined fixed frequencies such as 20 KHz, 30 kHz, or 40 KHz with an ultrasonic welder[4], or at lower power at arbitrary frequencies with a broadband piezoelectric stack[5]. The actual vibration of the specimen is dominated by resonance effects, and at high power the nonlinearity of the interaction between

the tip of the transducer and specimen can cause the generation of harmonics, sub-harmonics, and even chaos[6].

While there have been attempts in the past to investigate frequency dependence with multiple fixed frequency welder systems [7], the applicability of such results is very limited because, without operating at natural resonances of the specimen, it is almost impossible to estimate the vibrational stress field impinging on the crack. By using a broadband source we can find the natural resonances of the specimen and make use of the known mode shapes of flexural resonances to quantitatively evaluate vibrational stresses from laser vibrometry measurements [3]. In this paper, we develop a theory of the frequency dependence of the vibrothermographic effect and evaluate that theory based on experimental evidence.

Theory

In the previous work[2], heating has been observed and modeled approximately as a quadratic function of dynamics stress amplitude σ_d.

Here we hypothesize a simple model for the frictional power at a single contacting asperity (contacting area):

$$P_i = \mu_i N_i \cdot v_i \tag{1}$$

where μ_i is the friction coefficient at this contacting asperity, N_i is the normal force (including static force $N_{(s)i}$ and dynamic force $N_{(d)i}$) and v_i is the tangential velocity. Assuming that the normal force $N = N_s + N_d$ is proportional to static and dynamic stress $\sigma = \sigma_s + \sigma_d$ and v_i is proportional to dynamic strain rate $(d/dt)\epsilon_d$, which for harmonic vibration is itself a proportional to frequency times dynamics stress $f\sigma_d$. Now for a given excitation duration $t_2 - t_1$, the total energy converted into heat is the summation of energy from all the contacting asperities of the crack:

$$\begin{aligned} E_{total} &= \sum_i \int_{t_1}^{t_2} P_i \, dt \\ &\propto (t_2 - t_1)(\sigma^s + \sigma_d)\sigma_d f \end{aligned} \tag{2}$$

Eq. (2) indicates that the total frictional energy may exhibit linear dependence on excitation frequency and, depending on the relative significance of static versus dynamic normal stresses, linear to quadratic dependence on dynamic stress. Total energy is represented by the change of temperature at the crack measured by the calibrated IR camera. To test Eq. (2), we will instead fit to a power law model, Eq. (3), where ΔT is the measured temperature rise, A is a crack dependent coefficient of proportionality which varies from crack to crack, and see whether the exponents α and β in the power law model match the predictions of 1.0 for frequency and between 1.0 and 2.0 for dynamic stress.

$$\Delta T = A\sigma^\alpha f^\beta \tag{3}$$

This power law model is reasonable for fitting the measured data because no heat is generated at zero stress or zero frequency, and it has the similar form as the physical model above, Eq. (2). The power law model also has the advantage of being linear of α and β in logarithmic space:

$$\log(\Delta T) = \log(A) + \alpha \log(\sigma) + \beta \log(f) \tag{4}$$

Experiment

There are two sets of specimens being used in this experiment to determine the frequency dependence of vibrothermography. The two sets were prepared and tested independently, almost a year apart. Set A includes fourteen 152 × 25.4 × 12.7 mm bars of Inconel 718 alloy and one 152 × 25.4 × 12.7 mm bars of Titanium-6Al-4V alloy. Each bar has a semi elliptical surface crack at its center. Each crack was grown from an initial electro-discharge machining (EDM) notch in three point bending using a servohydraulic testing machine. R ratio was set

to 0.1 and the bending stress was 80% of the yield stress of the material. After initial crack growth of several thousand cycles, the specimen surface was machined removing the EDM notches and leaving only the fatigue crack underneath. Final crack lengths from Set A range from x mm to x mm.

The second set of specimens, called Set B, has two Titanium-6Al-4V alloy bars, with the geometry of 310 × 25.4 × 6.1 mm. The fatigue process was similar to Set A, except that each specimen was seeded with thirteen EDM notches and the specimens were fatigued in four point bending so as to apply equal load during fatigue. Nine and thirteen cracks were identified on specimens B1 and B2 respectively using optical microscopy. Of these, five and nine respectively were large enough to be detectable using vibrothermography. Locations of the cracks are shown in Figure 1. Off-center cracks tend to grow faster than cracks at the center, because the stress is higher off close to the edge due to the poisson's effect. TABLE 1 summarizes the crack lengths in Set A and Set B.

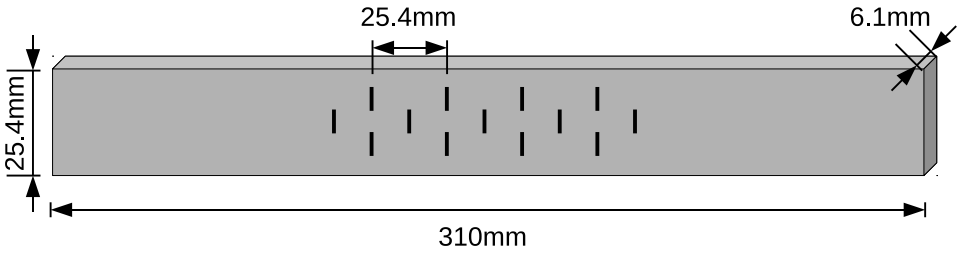

Figure 1: Crack locations of specimen in Set B. Thirteen notches (bold lines in the figure) were made. Five center cracks and eight off center cracks.

Table 1: Cracks length characteristics in Set A and Set B (all lengths are in mm)

	number of cracks	min length	max length	mean length	median length
Set A	15	0.56	8.64	2.14	1.68
Set B	14	1.78	5.44	3.08	2.87

The simplest way to load these cracks with known vibrational stresses at different frequencies is to make use of bending-mode flexural resonances that will apply normal opening/closing stresses on the crack. It is found through laser vibrometry measurements that when the specimen is mounted by using rubber pins at its vibrational nodes, both the resonance frequency and the mode shape match the frequency and shape for free vibration, calculated using finite-element techniques. Therefore, based on the assumption that the motion is adequately represented by the finite-element calculation, stress in the specimen is estimated by measuring a single point velocity and scaling by the stress/displacement ratio from the finite element calculation.

The finite element calculation was performed with an open source package called CalculiX [8]. For specimens in Set A, 16384 20-node brick elements were used, and for the specimens in Set B, 49152 elements of the same type were used. The grid independence study was performed by doubling the number of nodes in a new finer grid, results showed that the differences of eigenfrequencies between original and finer grids were less than 1% and differences of stress/displacement ratios were less than 2%.

The excitation system is shown in Figure 2. The specimens were excited at their flexural resonances using a piezoelectric stack actuator driven by a high power tone burst. Resonant frequencies varied slightly because of slight differences in geometry from specimen to specimen. Specimens in set A were excited at their 3rd and 5th order flexural resonance modes, near 13 KHz and 29 KHz respectively. Specimens in set B were excited at their 8th, 9th and 10th flexural resonance modes, near 10 KHz, 12 KHz and 15 KHz respectively. Infrared images of crack heating were captured using a calibrated infrared camera, and processed to estimate the temperature increase. For each specimen at each resonance mode, several data points were collected by varying the excitation amplitude in a predetermined random order.

Results

The finite element simulations of resonant modes were validated by comparing surface motion, as measured through scanning a laser vibrometer, with calculations from the simulation.

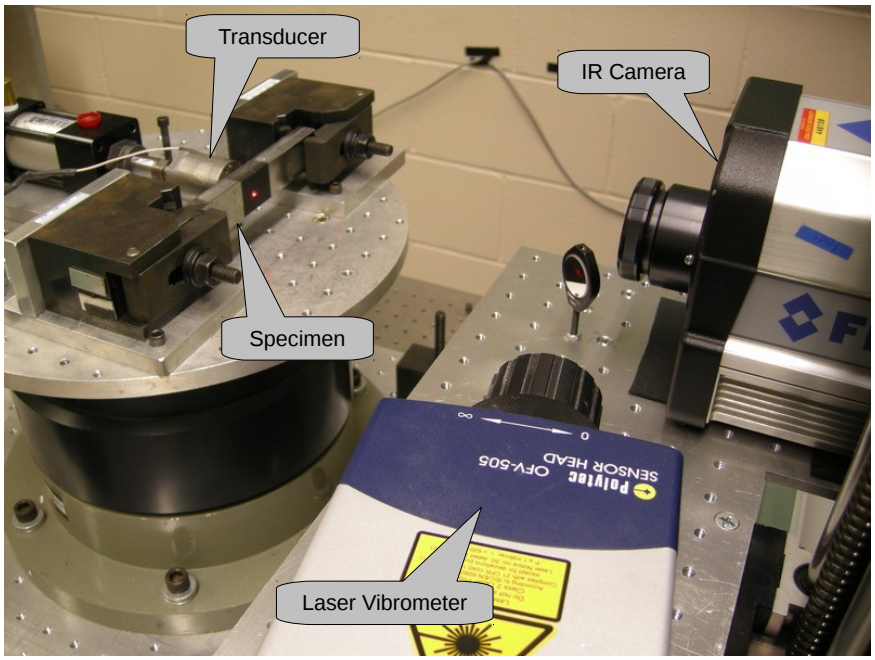

Figure 2: Experimental setup used for exciting the test specimens and observing heat generation.

Figure 3 shows the comparison between the experimental motion profiles (velocity or displacement) for specimen A114 from Set A at its 3rd, 4th and 5th flexural resonance modes and the calculated motion profiles from finite element. The amplitudes in Figure 3 have been scaled to match, and it is clear from the figure that the locations of nodes and anti-nodes agree well between experiment and theory.

At low frequency resonances, the vibrating specimen approximates the bending of a slender beam, and therefore elementary flexural wave theory[9] can be used as an additional check on the validity of the finite element calculation. In particular, it can be used at low frequencies as an independent measure of the stress/displacement ratios we will be using to estimate the vibrational loading on cracks. Figure 4 show that stress/displacement ratios calculated using

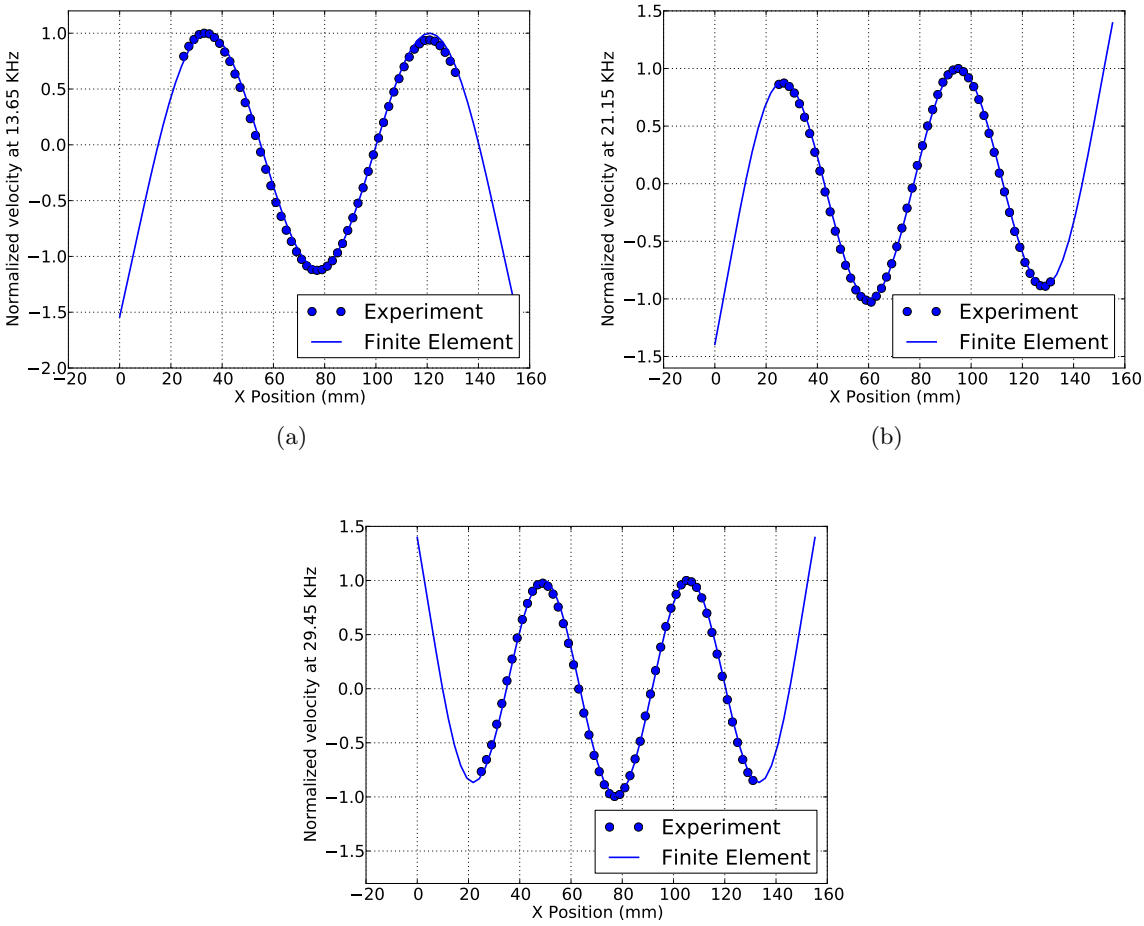

Figure 3: Comparison of surface velocity profile between laser vibrometer scanning and finite element simulation at different resonance modes.

finite element match those calculated from elementary theory at low frequency.

We tested all specimens in Set A and Set B at their different resonance modes. An example infrared image of a heating crack is included as Figure 5. Heating versus dynamic normal stress for several resonances on typical cracks from Set A and Set B are shown in Figure 6 and Figure 7 respectively. Figure 6(a) shows specimen A119 at its third (13.8 KHz) and fifth order (29.6 KHz) flexural resonances. Figure 6(b) Shows specimen A124 at its third (13.5 KHz) and fifth order (29.1 KHz) flexural resonances. Figure 7(a) shows the heating of crack B1_12 of specimen B1 at its eighth (9.8 KHz) and tenth order (14.5 KHz) flexural resonance modes. Figure 7(b)

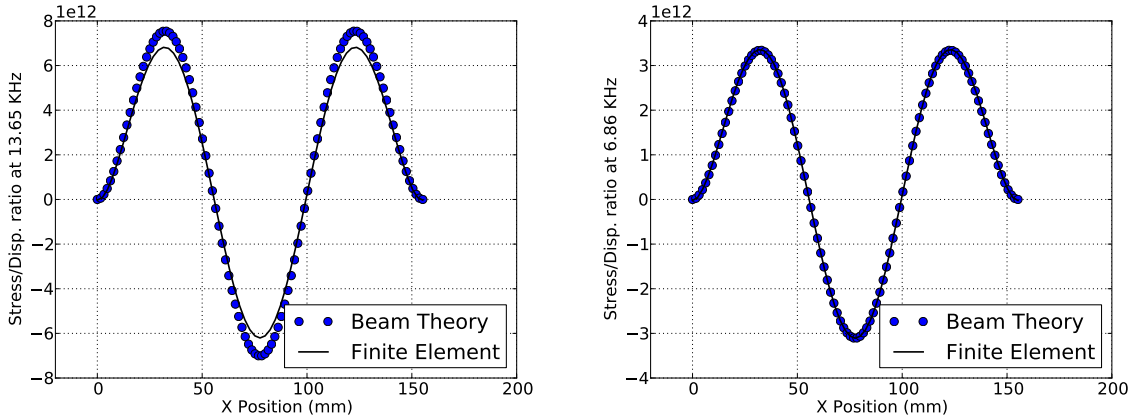

(a) (b)

Figure 4: Comparison of stress/displacement ratio between flexural beam theory and finite element simulation. (a) has the same geometry as the specimens in Set A, while (b) has half the thickness, which makes the resonance frequency lower and the result from flexural beam theory matches that from finte element.

shows the heating of crack B2_13 of specimen B2 at its nineth (12.4 KHz) and tenth (14.9 KHz) resonances. Because of the stress profiles at different resonances are different, cracks may not heat up at all resonances.

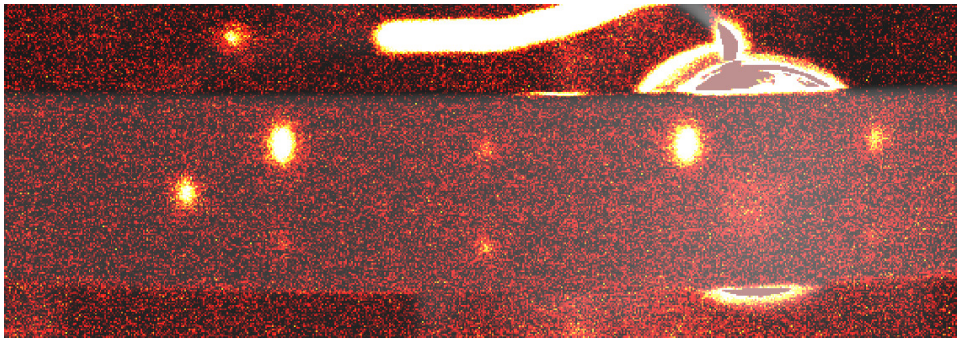

Figure 5: A typical vibrothermographic heating recorded by the calibrated infrared camera. This is specimen B2 from Set B.

The tool we used to fit the data to the power law model Eq. (3) is called the mixed effect

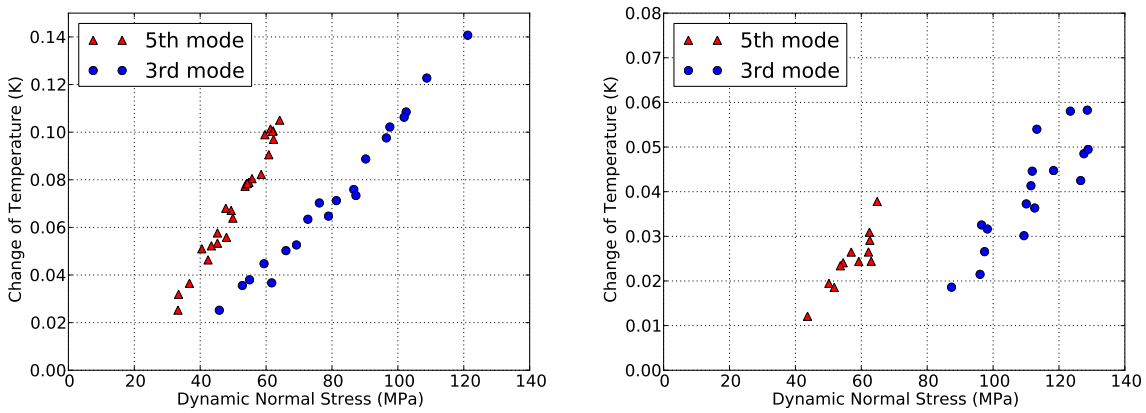

(a) (b)

Figure 6: Heating versus dynamic normal stress at two different resonances. These two specimens are A119 and A124 from Set A.

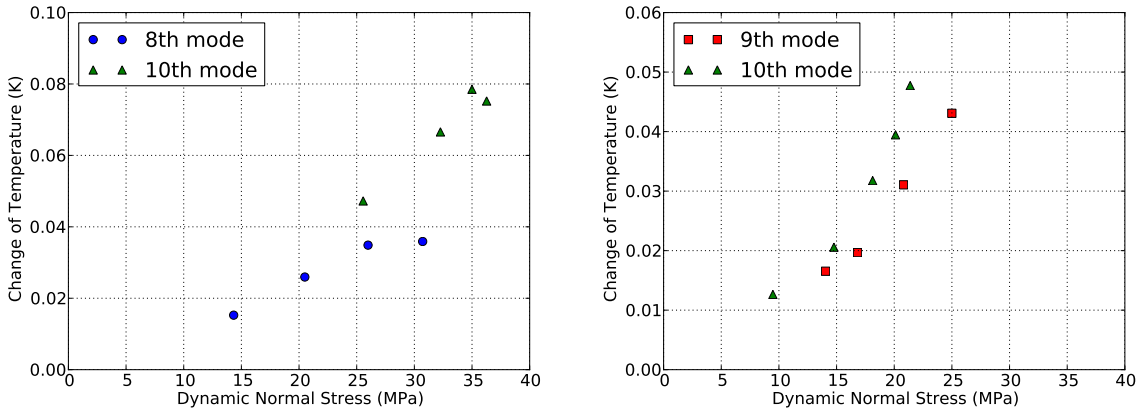

(a) (b)

Figure 7: Heating versus dynamic normal stress at different resonances. These two cracks were B1_12 on specimen B1, and B2_13 on specimen B2 from Set B.

linear regression[10], which is implemented in the open source statistical package *R*[11] as function *lmer()*. It is assumed that specimens in Set A and Set B are drawn randomly from a large population of specimens (cracks), each of which has a different observed value of the crack dependent coefficient $\log A$ (random effect), while the fixed variables α and β (fixed effects) are independent of cracks. We applied the mixed effect linear regression to two sets of specimens, and the estimated values are shown in TABLE 2.

Table 2: Estimated parameters from statistical models, with standard error

	$\log A$	α	β
Set A	-8.07 ± 0.24	1.73 ± 0.03	0.88 ± 0.04
Set B	-7.53 ± 0.58	1.88 ± 0.08	0.87 ± 0.13
combined	-7.73 ± 0.20	1.74 ± 0.03	0.88 ± 0.03

It is possible to visualize the fitted results for Set A and Set B in 3-D plots, as illustrated in Figure 8(a) and Figure 8(b). The corrected logarithmic temperature increases $\log(T/A)$ are plotted as functions of logarithmic stress and logarithmic frequency, and the planar surfaces are drawn from the fitted α and β. Since the surface is not completely opaque, data points below the surface are also visiable.

Conclusions

In this paper, we presented the measurement of frequency dependence of vibrothermographic heating, and by employing the simple but physically reasonable power law model, we estimated the quantitative relation between temperature rise, dynamic normal stress and excitation frequency.

We observe that the vibrothermographic heating $\Delta T \propto f^{0.88}\sigma^{1.74}$. Comparing with the physical model, the stress exponent α is close but not equal to 2. This indicates that in addition to the dynamic vibrational stress, some of the heating may also come from dynamic sliding against a static normal force, which would give linear dependence of heating on stress.

While the physical model predicts that heating is linear in frequency, our data shows that the frequency exponent β is 0.88. This suggests that the model has some validity, but does

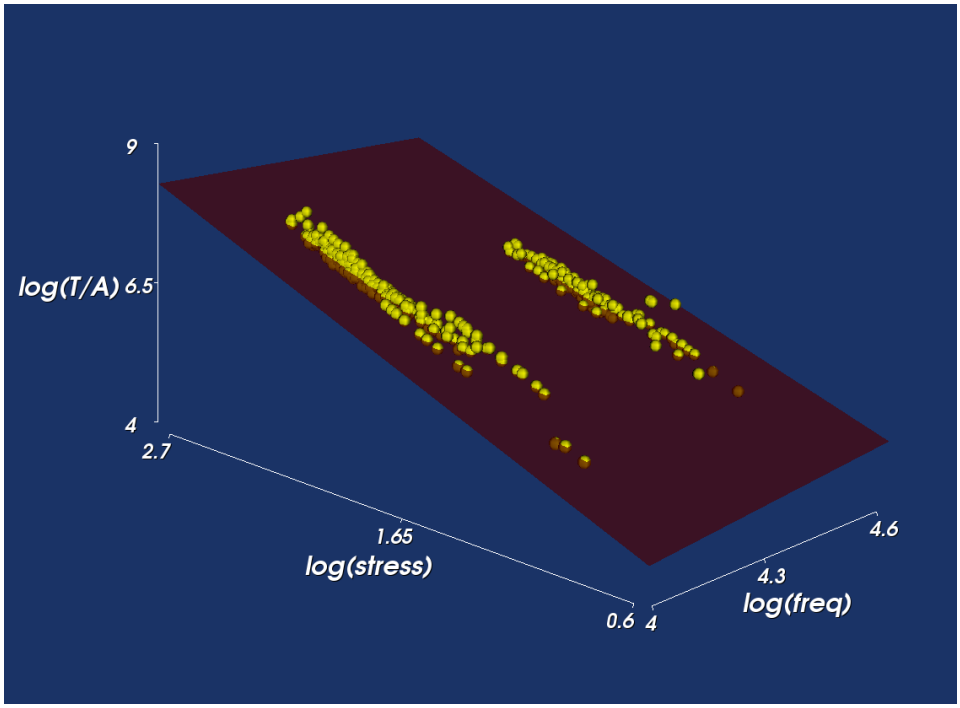

(a)

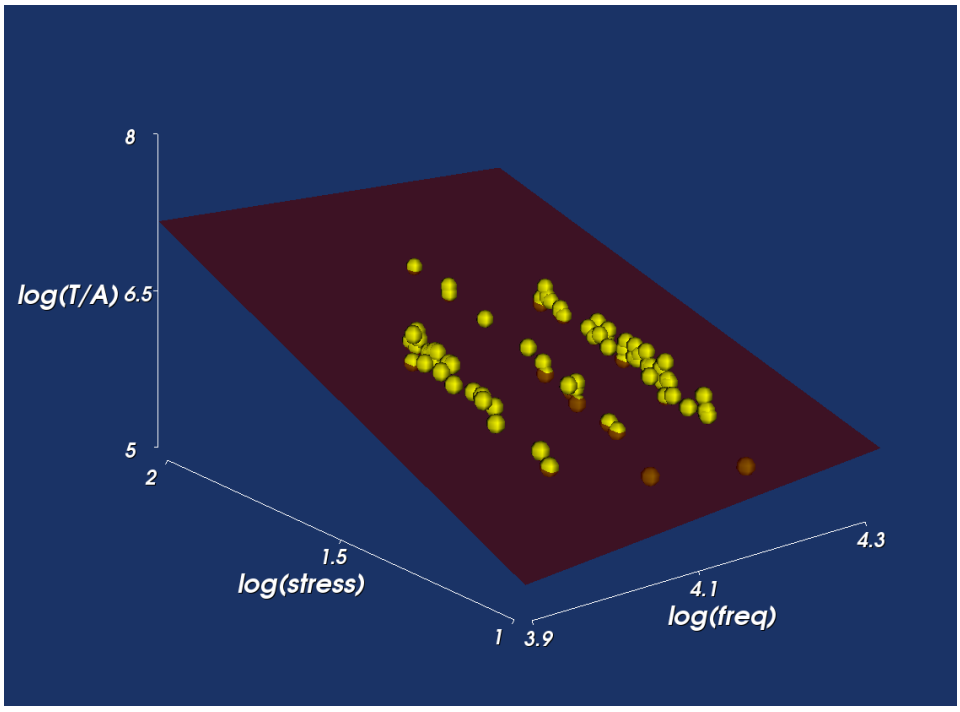

(b)

Figure 8: 3-D plots of the measured data points and the fitted surface. (a) shows the data from Set A, at two different resonances. (b) shows the data from Set B, at three different resonances.

not completely capture the physics of the frictional heating underlying vibrothermography.

Acknowledgements

This material is based upon work supported by the Air Force Research Laboratory under Contract #FA8650-04-C-5228 at Iowa State University's Center for NDE.

DEPENDENCE OF VIBROTHERMOGRAPHIC HEATING ON SHEAR VERSUS NORMAL LOADING

A paper to be submitted to NDT&E International

Wenjun Zhang and Stephen D. Holland

Abstract

Modal dependence of Vibrothermography is a long-standing question, and it has never been answered by researchers. We present here the first experimental data of the heat generated by fatigue crack under shear loading, and compare the heating due to normal loading. Experimental results show that both shear (Mode II/Mode III) vibration and normal (Mode I) vibration can cause crack heating, and in the power law model, the stress exponents in both cases are approximately 1.7.

Introduction

Vibrothermography, also known as sonic infrared and thermosonics, is a technique for finding cracks and flaws based on heat generated when a crack is vibrated. A specimen is excited with high power sonic or ultrasonic vibration, and the resulting rubbing of crack faces generates heat that flows to the surface and is imaged with an infrared camera [12, 4, 1].

Intuitively, one would expect such heating to be driven by shear on the crack surfaces; shear would create a motion velocity perpendicular to the normal forces generated by crack closure that directly translates to power dissipation $P = \mu N \cdot v$. Indeed, this has been tested for synthetic delaminations in composites and found to be true[13]. It has therefore long been

hypothesized that for cracks as well vibrothermographic heating is dominated by shear (*Mode II* or *Mode III*) loading In this paper we test the hypothesis that crack heating is dominated by shear, but find instead that amounts of crack heating are approximately the same for Mode II/III shear loading as they are for Mode I tension/compression.

The hypothesis of shear-driven heating would lead us to believe that little heating should occur when a crack is exposed exclusively to normal stress, compared with the same crack exposed to a similar amount of shear stress. In fact, when a specimen is exposed to the stress levels required to generate detectable vibrothermographic heat, our data shows similar amount of heating occurs due to both normal and shear stresses. In addition, when we fit a simple power law model to the heating we find dependence on normal stress of approximately $\sigma^{1.8}$, and dependence on shear stress of $\tau^{1.8}$.

Quantitatively evaluating vibrational loading on a crack is very difficult experimentally because of the inherent stress concentrations and the need not to block the infrared camera's view of the surface with, for example, a strain gage. Moreover, most experimental systems use powerful mono-frequency ultrasonic welders as excitation sources in order to transmit enough energy to cause detectable temperature changes. Because of the non-resonant, chaotic nature of the vibration, motion and dynamic stresses around the crack can not be accurately determined.

In these experiments we determine the dynamic vibrational stresses on the crack through a measurement that combines resonant mode excitation [14] with single-point motion measurements. The specimens are a simple bar geometry held softly with rubber pins so as not to perturb the natural resonances. The mode shapes are known from finite element calculation and validated experimentally through laser vibrometer scanning and observations of vibrothermographic heating of viscous adhesive coatings. Single point motion velocity measurements are performed with a laser vibrometer. The combination of known mode shape plus known point motion gives the vibrational engineering stresses everywhere inside the specimen.

By very careful specimen design, modal analysis, and experiment we were able to independently and separately apply pure normal vibrational stress ($\sigma \gg \tau$) and pure shear stress

($\tau \gg \sigma$) to the same crack, at different resonance modes. We find that both shear (Mode II/Mode III) vibration and normal (Mode I) vibration can cause crack heating, and surprisingly, their characteristics seem to be quite similar.

Theory

Assume the total frictional power generated by rubbing surfaces in a crack is the summation of the power from all contacting asperities:

$$P = \sum_i P_i = \sum_i \mu_i N_i \cdot v_i \tag{1}$$

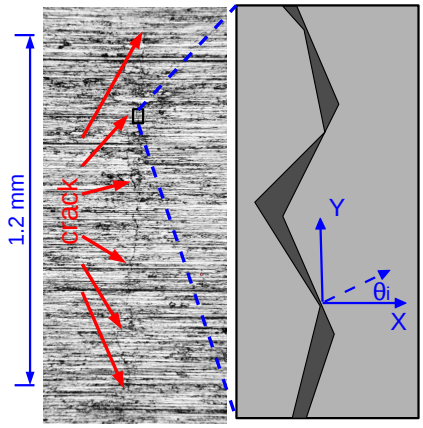

Figure 1: A typical 1.2 mm fatigue crack under optical microscopy (left) and the sketch of the contacting asperities (right). The local orientation is different in each of the contacting asperities. The remote stress is then decomposed into normal and shear component in these local contacting asperities.

While the crack has a unique orientation, the local contact angle is different at each contacting asperity, as illustrated in Figure 1. For an asperity angled at θ_i (plane stress), the average normal and shear dynamic stresses at the plane parallel to this contacting area are then[15]:

$$\begin{aligned} \sigma_i^d &= \frac{\sigma_x^d + \sigma_y^d}{2} + \frac{\sigma_x^d - \sigma_y^d}{2} \cos 2\theta_i + \tau_{xy}^d \sin 2\theta_i \\ \tau_i^d &= -\frac{\sigma_x^d - \sigma_y^d}{2} \sin 2\theta_i + \tau_{xy}^d \cos 2\theta_i \end{aligned} \tag{2}$$

Arguably, the lateral velocity v_i in Eq. (1) should be proportional to the angled dynamic shear strain rate $\dot{\gamma}_i^d$ (also $\dot{\tau}_i^d$ for linear elasticity). The normal force N_i however, should be proportional to sum of angled dynamic normal stress σ_i^d and static normal stress σ_i^s at that contacting asperity. With these relations, the frictional power in Eq. (1) becomes:

$$P(\sigma_x^d, \sigma_y^d, \tau_{xy}^d, \theta_i, \mu_i, \sigma_i^s, t) \propto \sum_i \mu_i (\sigma_i^d + \sigma_i^s) \cdot \dot{\tau}_i^d \tag{3}$$

In other words, the frictional power always has the product of static or dynamic stress and the time derivative of dynamic stress. If we restrict ourselves to the case of pure normal dynamic stress ($\sigma_x^d \gg \sigma_y^d, \tau_{xy}^d$) under harmonic motion ($e^{i2\pi ft}$), e.g. from a bending resonance, then the angled normal stress and shear stress rate are:

$$\begin{aligned} \sigma_i &= \frac{\sigma_x^d}{2} + \frac{\sigma_x^d}{2}\cos 2\theta_i + \sigma_i^s \\ \dot{\tau}_i^d &= -i2\pi f \frac{\sigma_x^d}{2}\sin 2\theta_i \end{aligned} \tag{4}$$

and therefore, the power in pure normal dynamic stress is:

$$\begin{aligned} P \propto\ & f(\sigma_x^d)^2 \sum_i \mu_i \left|\sin 2\theta_i (1 + \cos 2\theta_i)\right| \\ & + f(\sigma_x^d) \sum_i 2\mu_i \left|\sigma_i^s \sin 2\theta_i\right| \end{aligned} \tag{5}$$

Similarly, in the case of pure shear dynamic stress ($\tau_{xy}^d \gg \sigma_x^d, \sigma_y^d$), the frictional power:

$$\begin{aligned} P \propto\ & f(\tau_{xy}^d)^2 \sum_i \mu_i \left|\sin 2\theta_i \cos 2\theta_i\right| \\ & + f(\tau_{xy}^d) \sum_i \mu_i \left|\sigma_i^s \cos 2\theta_i\right| \end{aligned} \tag{6}$$

This model, Eq. (5) and Eq. (6), predicts that depending on the relative significance of static and dynamic stress, vibrothermographic heating exhibits linear to quadratic dependence on dynamic stress, regardless of the type of dynamic loading (normal or shear). The following sections are experimental validations of this new explanation.

Experiment

The specimen geometry was selected so that there could be cracks in individual locations under normal stress at one vibrational resonance and shear stress at another resonance. After

finite element simulation and experimental validation, we selected two 310 × 25.4 × 6.1 mm bars of Titanium-6Al-4V alloy. For each of the two bars, fatigue cracks were grown from thirteen initial electro-discharge machining (EDM) notches in four point bending using a servo hydraulic testing machine. The maximum bending stress was set to 80% of yield stress and the R ratio (min/max stress) was 0.1, at frequency 1 Hz. The specimen surfaces were ground after several thousand cycles, removing the EDM notches but leaving the cracks underneath. Each specimen was then fatigued until at least one crack approached a critical length. The crack growth rates vary, so final crack lengths range from 15 mm to 214 mm. After the fatigue process, five and ten cracks in specimens A and B respectively were long enough to be detected with vibrothermography technique, although twenty-two out of twenty-six cracks were found under optical microscopy. Coordination and cracks are sketched in Figure 2.

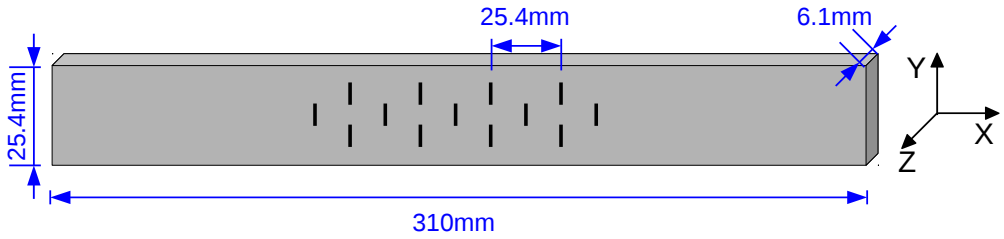

Figure 2: Specimen with multiple initial EDM notches and fatigue cracks. There are five center notches and eight off center notches on each specimen. Horizontal distance between the neighboring two notches is 25.4 mm and the vertical distance between two notches is 12.7 mm. Fatigue cracks were grown from these notches.

A simple but effective way to apply normal and shear stress on the specimen is flexural resonance. Finite element simulation and elementary theory show that when the specimen is vibrated in free flexural resonance around the Z axis, all cracks are loaded in tension and compression. In contrast when the specimen is vibrated in free flexural resonance vibration around Y axis, as shown in Figure 3, cracks at the center (neutral line) are loaded in pure shear, while off center cracks may be loaded in the combination of normal and shear (mixed mode), depending on their location and the resonance. In the experiment, heating data from

all cracks was collected, but only that from center cracks, where pure shear loading could be achieved, was used in the analysis for the shear stress dependence.

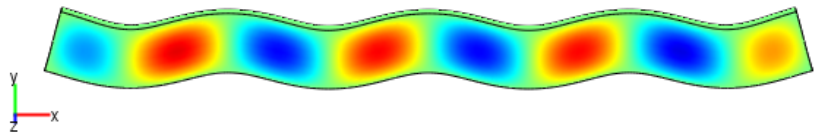

(a)

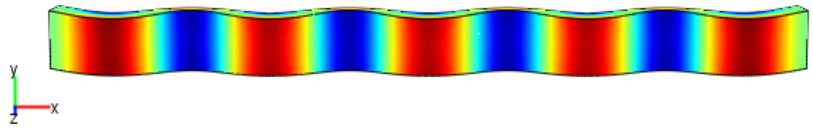

(b)

Figure 3: Flexural resonances in two directions. Vibration shown in (a) is in the Y direction, and the color is mapped from dynamic shear stress. Vibration in (b) is in Z direction (out of the paper), and the color is mapped from dynamic normal stress.

The excitation system to create shear loading is shown in Figure 4. The specimen is held by two small pieces of rubber sheet at its vibrational nodes as not to perturb the free vibration. A Piezoelectric transducer excites the specimen at its anti-node to create flexural resonant vibration. Given the known mode shape from finite element simulation and single point velocity from laser vibrometer measurement, dynamic stresses in the specimen can be estimated by simply multiplying the displacement (integral of measured velocity) with a stress/displacement factor from finite element simulation. During the measurements, we found that the laser vibrometer tape, which was intended to increase the signal quality of the vibrometer, also generates heat when loaded. This effect provides direct indication of the vibration modes, as illustrated in Figure 5. To apply normal (tension/compression) loading on cracks, the setup is similar except that the transducer is placed at the back of the specimen instead of on the top as seen in Figure 4.

Although the resonance frequency and the heating pattern from the vibrometer tape agree well with the finite element simulation, a slight amount of undesired motion was observed. We mounted a second vibrometer to measure motions normal to the desired resonance being

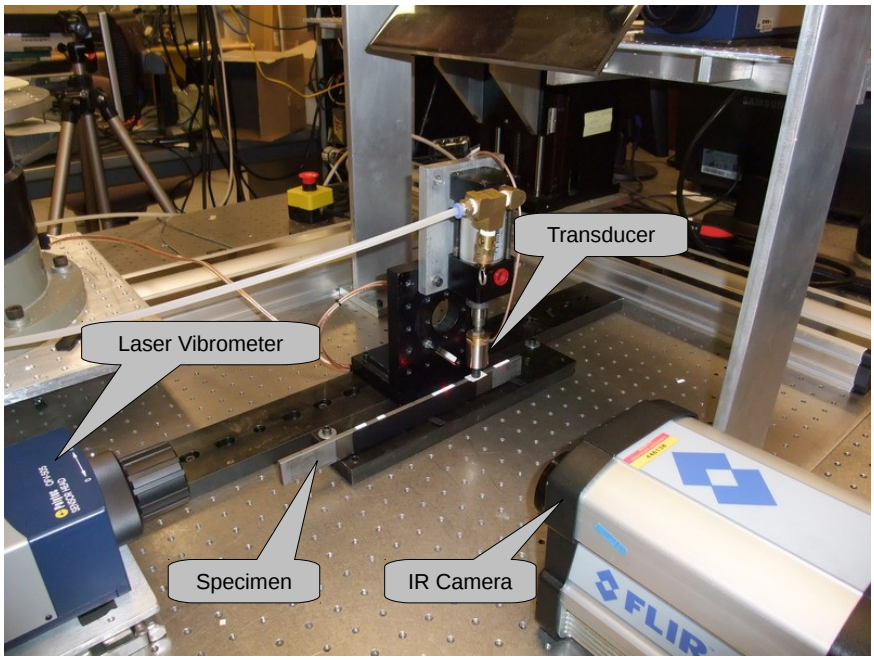

Figure 4: Experimental setup in this study. Piezoelectric transducer excites the flexural vibration in the vertical direction, motions were measured by laser vibrometers, and the heating was recorded by the infrared camera.

excited, which could come from bending in the other axis and/or torsion. The velocity amplitude of these unwanted motions were observed to be less than 10% of the stress amplitude from the desired resonance, and given that the stiffness is much higher when bending in the Y direction, any induced normal stresses must be far less and negligible.

In the experiment, tone burst excitation at their 7th order flexural resonance (Y direction), as well as 8th, 9th and 10th order flexural resonance (Z direction) were used. The former gives pure shear stress at center cracks, and the latter gives normal stress at all cracks. Temperature change from the all the cracks were recorded by a calibrated infrared camera, and the dynamic stresses at those cracks were calculated later from the laser vibrometer measurement of the

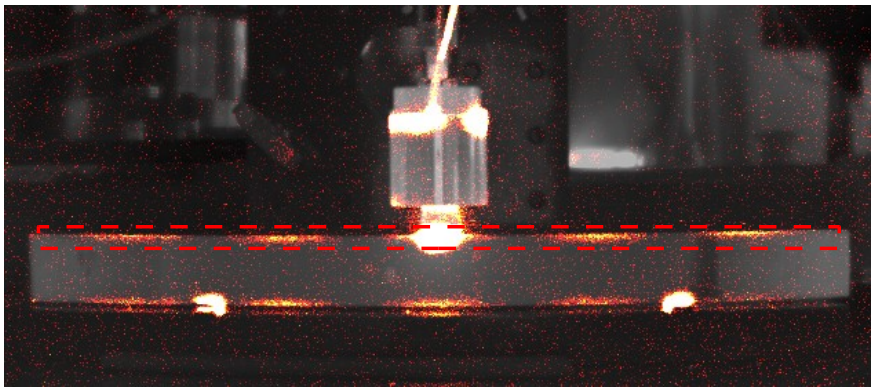

Figure 5: Heating of the vibrometer tape. Tapes were stuck to the top and the bottom of the specimen. This heating pattern indicates the 5th order flexural resonance mode. The two brigher spots at the bottom of the specimen were rubber pins, which were placed at the nodal points.

velocity. By varying excitation amplitude, temperature rises at different dynamic stresses were recorded and analyzed.

Results

Four center cracks (see Figure 2) were detected under moderate stress level with the infrared camera, as shown in Figure 6 and Figure 7. One may notice that in Figure 7, there is no such heating patterns from the laser vibrometer tape, as shown in Figure 5. The reason is that we removed the tapes as to prevent interference in the temperature measurement of the cracks. But the mode shapes were validated by other means for this specimen in this configuration. It is also seen that heating from some cracks are significantly stronger than the other, beside the differences in stress status, those cracks are usually larger than the others.

To test the validity of Eq. (5) and (6), we defined our statistical model to be:

$$\Delta T_{ij} = A_i \ \sigma_{ij}^{\alpha} \ f_{ij}^{\beta} \ e^{\epsilon_{ij}} \tag{7}$$

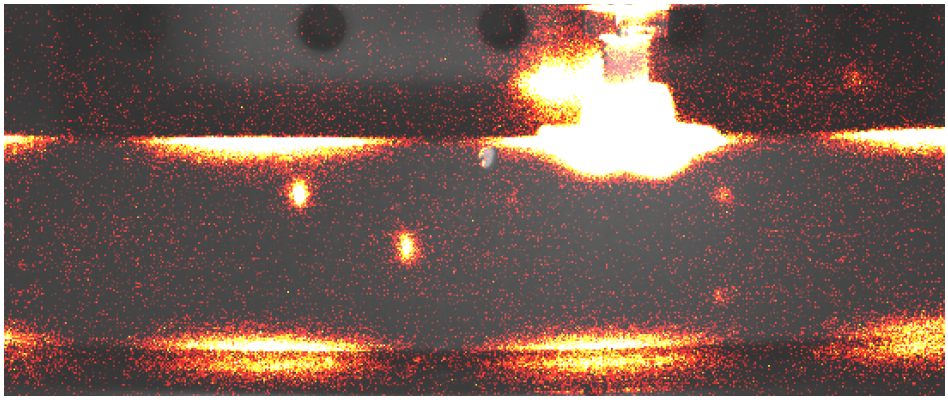

Figure 6: Vibrothermographic heating from cracks in specimen B1. Five cracks can be identified from this figure, but only the one in the middle was under pure shear dynamic stress.

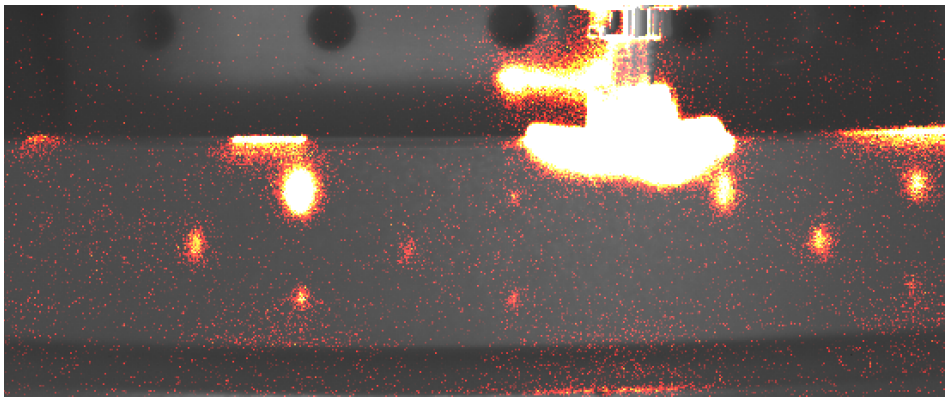

Figure 7: Vibrothermographic heating from cracks in specimen B2. Ten cracks can be identified from this figure, and the three along the center line were under pure shear dynamic stress.

where ΔT is the change of temperature, which is a representation of the total frictional power (or energy over the excitation duration), σ is the amplitude of dynamic normal or shear stress, A is the proportionality coefficient, α and β are the exponents of stress and excitation frequency f, as in Eq. (5) and (6), and ϵ is the error. Subscripts i and j represent the jth measurement of the ith crack. Value of β was first determined from the cracks under normal stress, and then substituted into the model of shear stress.

After taking logarithm on both sides, $\log(\Delta T)$ became a linear function of $\log \tau$, with the slope α and intercept $\log A$. We employed the mixed effect linear model[10] in the statistics package R[11] to deal with data such as this where some parameters ($\log A$) are grouped (per-crack) and others are common to all cracks (α and β), and treated $\log A$ as a random variable with mean and variance across the whole population of cracks (not only the four cracks here). Another advantage of the mixed effect model is that it greatly reduces the number of parameters to be estimated. For the cracks under pure normal stress, the estimated population mean of $\log A$ is -7.53, with standard error 0.58, the estimated exponent α of normal stress is 1.88 with standard error 0.08, and the estimated β is 0.88, with standard error 0.03, which agree well with the previous observations [16]. Now the statistical model for cracks under pure shear becomes:

$$\log \Delta T_{ij} = \log A_i + \alpha \log \tau_{ij} + 0.88 \log f_{ij} + \epsilon_{ij} \tag{8}$$

The estimated exponent α of dynamic shear stress is 1.74, with standard error 0.067, and the estimated population mean of the $\log A$ is -7.53, with standard error 0.14.

It is also possible to use the normal linear regression method to fit the data, which directly provides the estimations of the four $\log A$s. As mentioned before, the drawback of this is that one cannot make inference on the heating other than these four cracks, and the increasing number of parameters may be an issue especially when sample size is small. In our case however, there is no much difference on the estimated value of α and β between two methods. The data and the fitted curves are shown in Figure 8, by substituting all the fitted parameters from the regular linear regression back to the model.

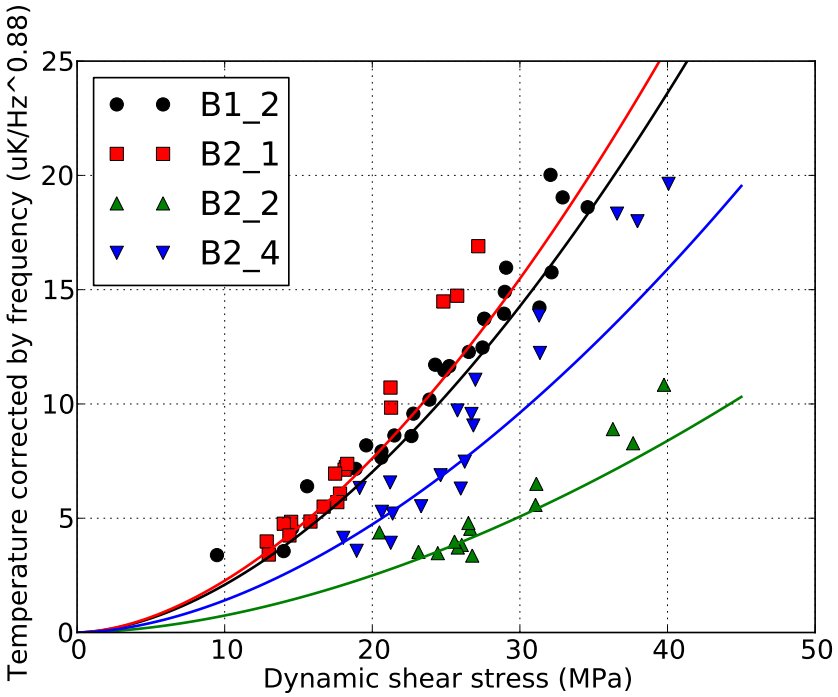

Figure 8: Temperature rises of the four center cracks versus dynamic shear stresses. Y axis in the plot is the temperature corrected by frequency, e.g. $\Delta T/f^{0.88}$.

Conclusions

To conclude, we presented the first controlled measurement of vibrothermographic heating under shear dynamic stress, and also quantified the exponent of shear stress in the power law heating model. Our measurements show that the heatings from normal or shear loading are quite similar, in fact, the stress exponent in both cases are approximately 1.7.

Also, we provided a simple physical model to explain this similarity. If one decomposes the dynamic stress into normal and shear components, and assumes that the normal force is proportional to the normal stress, and the tangential velocity is proportional to the shear stress, than the frictional power, will have this quadratic dependence on dynamic stress, regardless whether it is normal or shear stress.

The exponents of stress in both cases are close but not equal to 2, one important reason is the existence of the static force at the contacting asperities, which introduces the linear dependence on dynamic stress. This is also a remaining topic in the future research.

Acknowledgements

This material is based upon work supported by the Air Force Research Laboratory under Contract #FA8650-04-C-5228 at Iowa State University's Center for NDE.

APPENDIX: PROCEDURE OF GROWING MULTIPLE CRACKS ON ONE SPECIMEN

Introduction

The motivation of making specimens with multiple cracks is to have similar cracks at different locations of a single specimen, so that more resonance modes can be used in the vibrothermography test. It also has the advantage in terms of saving time and material. The procedure of growing multiple cracks is similar to the procedure of growing single crack on one specimen, which is being used here in the Center for NDE.

Growing multiple crack is more difficult and needs more careful monitoring. There are two main issues: 1) cracks will nucleated and initiated differently, according to the micro structure and material properties; 2) once one crack is longer than the others, it will unload the others cracks, prevent others from growing and become more and more dominant.

To minimize the interaction between neighboring cracks, Prof. Bastawros suggests that the separation between cracks should be larger then at least 5 times of the size of the plastic zone. A simple calculation is provided to estimate this length.

For a semi-circle surface crack with crack length $2a$ and depth a, the stress intensity factor [17]:

$$K_I = 1.144\sigma\sqrt{\frac{\pi a}{2.464}} \tag{9}$$

According to Irwin approximation of the plastic zone size[18], the monotonic plastic zone size for plane stress is about (cyclic plastic zone is smaller than monotonic plastic zone):

$$r_p = \frac{1}{\pi}\left(\frac{K_I}{\sigma_{yield}}\right)^2 \tag{10}$$

In the fatigue process, $\sigma = 0.8\sigma_{yield}$, then substituting everything into the plastic zone expression, we have

$$r_p = 0.33a \tag{11}$$

For example if $a = 1mm$, theoretically as long as the separation between two neighboring crack tips is more than $5mm$, interaction between cracks can be ignored, which ensures the possibility of making multiple cracks in one specimen.

Four point bending was used in stead of three point bending, as to apply the same dynamic loading to all cracks. The bending stress is constant within the inner spans in four point bending, and it is function of applied force F, length between loading span and supporting span a, width b and thickness d of the specimen:

$$\sigma = \frac{3Fa}{bd^2} \tag{12}$$

We selected a low R-ratio (0.1) in the hope that the large change in stress would give consistent crack growth per cycle. Bending stress was set to 80% of the yield stress of the specimen in fatigue crack growth process, in order the lower the number of total cycles, minimizing the scatter caused by time-to-initiate.

Step-by-step procedure

- STEP 1: Surface preparation

  Specimens may come with residual stress, oxidation and scratches on the surface, and grinding provides an appropriate surface for crack initiation. Also, with a smooth surface, crack growth can be monitored under optical microscopy more easily.

- STEP 2: EDM starter notch

  Electrical Discharge Machining (EDM) notches induces stress concentration at the tip of the notch, which helps the crack to initiate. It may be better to make these notches as identical as possible. (but I didn't find any correlation between the final crack length and the size of the starter notch.) However, even though the settings remain the same, the electrode can ware and as a result, making the length and depth of the later notches

differ from the older ones. Since the specimen is submerged in the dielectric fluid during machining, it needs to be cleaned and dried before fatigue, usually using aceton in the ultrasound cleaner for cleaning and oven at 150 F for drying.

- STEP 3: First crack growth

  Fatiguing is done by the servohydraulic machines in CNDE. Carefully mount the specimen onto the bending fixture and input the proper parameters (Mean Load, Amplitude, Frequency, etc.) in the control software. It is found that the machine cannot reach the desired force when the frequency is too high (for example 5 Hz). Therefore I used 1 Hz for all the specimens with multiple cracks. With the bending stress at 80% of yield, fatigue cracks will show up at the tips of the starter notches, usually from few thousand cycles. Check the crack length every 2000 cycles under microscopy.

- STEP 4: Removing EDM notches

  Keep fatiguing the specimen until cracks show up from all notches and their lengths are more than the twice the depth of the starter notches (ideal), or until some of the cracks being too long (reality), then grind the surface again. The purpose is to remove the EDM notches and leave only the fatigue crack. Dr. Jeremy Renshaw suggested that machining off twice the depth of the starter notch to remove the effect of the heat affected zone as well.

- STEP 5: Final crack growth

  Mount the specimen back to the fixture, and repeat the fatiguing until the crack lengths reach the designed value. Unmount the specimen and check the length of the cracks under optical microscopy every 2000 cycles.

Summary

Sizes of the notches and cracks of specimen B1 and B2 are shown in Table 1.

Table 1: Size of EDM notches and final length of cracks of specimen B1 and B2 (all lengths are in mm)

ID	Specimen B1 (24430 cycles)				Specimen B2 (38000 cycles)			
	Notch			crack	Notch			crack
	length	width	depth	length	length	width	depth	length
1	0.508	0.034	0.095	1.60	0.521	0.079	0.027	4.27
2	0.533	0.053	0.099	3.25	0.521	0.079	0.026	2.37
3	0.559	0.030	0.085	1.14	0.521	0.079	0.028	1.80
4	0.533	0.034	0.085	0.58	0.521	0.069	0.026	3.15
5	0.533	0.030	0.089	0	0.495	0.079	0.028	1.07
6	0.523	0.034	0.089	0	0.508	0.079	0.024	2.13
7	0.533	0.045	0.095	0.38	0.508	0.079	0.025	2.13
8	0.533	0.047	0.089	2.03	0.521	0.079	0.027	0.94
9	0.533	0.030	0.086	0	0.508	0.079	0.027	1.98
10	0.533	0.045	0.091	3.05	0.533	0.059	0.026	5.44
11	0.533	0.045	0.091	1.78	0.533	0.069	0.024	2.13
12	0.533	0.041	0.089	2.69	0.521	0.050	0.028	4.95
13	0.544	0.030	0.086	0	0.508	0.079	0.026	3.73

BIBLIOGRAPHY

[1] X.P.V. Maldague. *Theory and Practice of Infrared Technology for Nondestructive Testing*. Wiley New York, 2001.

[2] Stephen D. Holland, Christopher Uhl, and Jeremy Renshaw. Vibrothermographic crack heating: A function of vibration and crack size. *AIP Conference Proceedings*, 1096(1):489–494, 2009.

[3] J. Renshaw and S.D. Holland. Full-field vibration measurement for vibrothermography. In *34th Annual Review of Progress in Quantitative Nondestructive Evaluation. AIP Conference Proceedings*, volume 975, pages 498–503, 2008.

[4] LD Favro, X. Han, Z. Ouyang, G. Sun, H. Sui, and RL Thomas. Infrared imaging of defects heated by a sonic pulse. *Review of scientific instruments*, 71:2418, 2000.

[5] S.D. Holland. First Measurements from a New Broadband Vibrothermography Measurement System. In *Review of Progress in Quantitative Nondestructive Evaluation; Volume 26 A(AIP Conference Proceedings Volume 894)*, volume 894, pages 478–483. American Institute of Physics, 2 Huntington Quadrangle, Suite 1 NO 1, Melville, NY, 11747-4502, USA,, 2007.

[6] X. Han, W. Li, Z. Zeng, LD Favro, and RL Thomas. Acoustic chaos and sonic infrared imaging. *Applied Physics Letters*, 81:3188, 2002.

[7] X. Han. Frequency dependence of the thermosonic effect. *Review of Scientific Instruments*, 74:414, 2003.

[8] G.D.C. Dhondt. *The finite element method for three-dimensional thermomechanical applications*. John Wiley & Sons Inc, 2004.

[9] W.C. Elmore, W.C. Elmore, and M.A. Heald. *Physics of waves*. Dover Pubns, 1985.

[10] Jose C. Pinheiro and Douglas M. Bates. *Mixed-effects models in S and S-PLUS*. Statistics and Computing. Springer, 2000.

[11] R Development Core Team. *R: A Language and Environment for Statistical Computing*. R Foundation for Statistical Computing, Vienna, Austria, 2010. ISBN 3-900051-07-0.

[12] E.G. Henneke, K.L. Reifsnider, and W.W. Stinchcomb. Thermography-An NDI method for damage detection. *Journal of Metals*, 31(9):11–15, 1979.

[13] KL Reifsnider, EG Henneke, and WW Stinchcomb. The mechanics of vibrothermography. *Mechanics of nondestructive testing*, pages 249–276, 1980.

[14] S.D. Holland, C. Uhl, and J. Renshaw. Toward a viable strategy for estimating vibrothermographic probability of detection. In *Review of Progress in Quantitative Nondestructive Evaluation*, volume 975, pages 491–497, 2008.

[15] William Franklin Riley, Leroy D. Sturges and Don H. Morris. *Mechanics of materials*. John Wiley, sixth, illustrated edition, 2006.

[16] W. Zhang, S.D. Holland, and J. Renshaw. Frequency Dependence of Vibrothermography. In *Review of Progress in Quantitative Nondestructive Evaluation*, volume 1211, page 505, 2010.

[17] T.L. Anderson. *Fracture mechanics: fundamentals and applications*. CRC, 2005.

[18] S. Suresh. *Fatigue of materials*. Cambridge Univ Pr, 1998.